PTCDA Molecular Monolayer on Pb Thin Films: An Unusual math xmlns="http://www.w3.org/1998/Math/MathML" display="inline">mi>π/mi>/math>-Electron Kondo System and Its Interplay with a Quantum-Confined Superconductor

Shuangzan Lu, Hyoungdo Nam, Penghao Xiao, Mengke Liu, Yanping Guo, Yusong Bai, Zhengbo Cheng, Jinghao Deng, Yanxing Li, Haitao Zhou, Graeme Henkelman, Gregory A. Fiete, Hong-Jun Gao, Allan H. MacDonald, Chendong Zhang, and Chih-Kang Shih

Phys. Rev. Lett. **127**, 186805 — Published 29 October 2021

DOI: 10.1103/PhysRevLett.127.186805

PTCDA molecular monolayer on Pb thin films: An unusual π-electron Kondo system and its interplay with a quantum-confined superconductor

Shuangzan Lu[1], Hyoungdo Nam[2], Penghao Xiao[3#], Mengke Liu[2], Yanping Guo[1], Yusong Bai[1], Zhengbo Cheng[1], Jinghao Deng[1], Yanxing Li[2], Haitao Zhou[4], Graeme Henkelman[3], Gregory A. Fiete[5,6], Hong-Jun Gao[4], Allan H. MacDonald[2], Chendong Zhang[1*] and Chih-Kang Shih[2*]

[1]*School of Physics and Technology, Wuhan University, Wuhan 430072, China*
[2]*Department of Physics, the University of Texas at Austin, Austin, TX 78712, USA*
[3]*Department of Chemistry, the University of Texas at Austin, Austin, TX 78712, USA*
[4]*Institute of Physics, Chinese Academy of Sciences, Beijing 100190, China*
[5]*Department of Physics, Northeastern University, Boston, MA 02115, USA*
[6]*Department of Physics, Massachusetts Institute of Technology, Cambridge, MA 02139, USA*
[#]*Present address: Materials Science Division, Lawrence Livermore National Laboratory, Livermore, California 94550, USA*
cdzhang@whu.edu.cn (C.D.Z) *shih@physics.utexas.edu (C.K.S.)*

The hybridization of magnetism and superconductivity has been an intriguing playground for correlated electron systems, hosting various novel physical phenomena. Usually, localized *d*- or *f*-electrons are central to magnetism. In this study, by placing a PTCDA (3,4,9,10-perylene tetracarboxylic dianhydride) molecular monolayer on ultra-thin Pb films, we built a hybrid magnetism/superconductivity (M/SC) system consisting of only *sp* electronic levels. The magnetic moments reside in the unpaired molecular orbital originating from interfacial charge-transfers. We reported distinctive tunneling spectroscopic features of such a Kondo screened π-electron impurity lattice on a superconductor in the regime of $T_K >> \Delta$, suggesting the formation of a two-dimensional bound states band. Moreover, moiré superlattices with tunable twist angle and the quantum confinement in the ultra-thin Pb films provide easy and flexible implementations to tune the interplay between the Kondo physics and the superconductivity, which are rarely present in M/SC hybrid systems.

The combination of magnetism and superconductivity, which are normally mutually exclusive, provides an intriguing platform involving rich quantum phenomena, such as the Yu-Shiba-Rusinov (YSR) bound states [1-3], the topological superconductivity harboring exotic Majorana modes [4,5], and the heavy-fermion behavior [6,7]. Among the hybrid systems experimentally explored thus far, magnetism is mostly derived from unpaired *d*- or *f*- electrons in transition metal atoms. Compared with *d*/*f* electrons, the *s*/*p*-electrons show distinctively different behaviors, such as more delocalized wavefunctions (therefore, larger spin correlation lengths) [8] and hyperfine spin-orbit couplings [9,10]. The creation of magnetic properties by π-electrons has attracted significant interest, which is expected to exhibit improved performance in spin-based information processing [10,11]. Various attempts have been made to achieve magnetism in graphene nanostructures by introducing sublattice imbalance [12-15] or topological frustration [16,17]. Also, charge transfer is another approach to introduce unpaired π-electrons in pure-organic molecules [18-20]; however, it has strict requirements on the work-function matching. Thus, only scarce examples were reported so far. By either of these two approaches, π-electron magnetic moments associated with a superconductor have not yet been realized. Moreover, few strategies were known to readily tune the π-electron magnetism, limiting the in-depth explorations to novel physics within variable regimes of the moment concentrations and the interaction strengths.

Here, we report a hybrid bilayer system comprised of a monolayer (ML) of the organic molecule (3,4,9,10-perylenetetracarboxylic-dianhydride, *i.e.,* PTCDA) and a superconducting Pb thin film. Although none of these two materials contains magnetism, surprisingly, we found that net spin moments formed in the molecular film, resulting in Kondo resonances near the Fermi level. First-principle calculations support the formation of spin-polarized lowest unoccupied molecular orbital (LUMO) states induced by interlayer charge transfer. By scanning tunneling spectroscopy investigations, we revealed distinctive characteristics of the combination of a Kondo screened π-orbital impurity lattice and a superconductor. In particular, our studies suggest the formation of a two-dimensional (2D) Kondo-induced impurity band near the superconducting gap edge. More interestingly, we found twistable moiré superlattices forming in this bilayer system, leading to moiré modulations for the Kondo-superconductivity interplay. In addition, the quantum confinement effect in Pb films provides another tuning knob to the charge transfer induced magnetic moments. These two appealing features combine in a single sample system, manifesting versatile tailoring of the complex interactions at the M/SC interface.

Figure 1(a) is a scanning tunneling microscopy (STM) image showing a crystalline PTCDA layer formed on a Pb(111) film (23 ML here), which is grown epitaxially on Si(111) (Methods in [21]). The herringbone structure of a PTCDA layer has a rectangular unit cell with unit vectors $\vec{a}_1$ = 1.29 ± 0.02 nm and $\vec{a}_2$ = 1.81 ± 0.02 nm. The angle between $\vec{a}_1$ and Pb<$1\bar{1}0$> is defined as θ in the inset of Fig. 1(a). In Fig. 1(b), we show a typical

tunneling spectrum (blue curve) taken on the ML PTCDA/Pb(111) film at a sample temperature T_S above the T_C of Pb film. A resonance peak appears at the Fermi level. The superconducting gap can coexist with this resonance peak (grey curve) when $T_S < T_C$. Based on the temperature dependence of the resonance [21] and its interplay with the superconductivity, we believe this resonance resulted from the Kondo effect. Note that the monolayer PTCDA with the herringbone structure can form on many metallic surfaces, yet no study has reported the observation of Kondo resonances in the pristine molecular film [20,45]. To support this hypothesis, we grew a PTCDA monolayer on the Ag(111) surface and found that the Kondo resonance was absent [red curve in Fig. 1(b)]. In addition, the Kondo resonance was absent for a single molecule on the Pb film [green curve in Fig. 1(b)] but emerged only after in-plane molecular hybridization occurred.

To understand the origin of the local magnetic moment, we performed DFT calculations for a single PTCDA molecule/Pb(111), ML PTCDA/Pb(111), and ML PTCDA/Ag(111) [21]. In Fig. 1(c), we plot the charge transfer and the magnetic moment for each molecule as a function of the interlayer separation d for all three systems. The calculations show a result consistent with the experimental observation that only monolayer PTCDA on Pb(111) possesses magnetic moments at the equilibrium distance (marked by vertical dashed lines). Figure 1(d) shows the partial density of states (DOS) of ML PTCDA/Pb at four interlayer separations d. As shown, the intra-orbital Coulomb repulsion energy U, the impurity state (*i.e.,* singly occupied LUMO) bandwidth W, and energy level (ε_{imp}) all varied with d. Note

that the LUMO states comprise relatively delocalized *s* and *p* electrons, leading to a small magnitude of $U \sim 0.1$ eV, which is comparable to the W and $\varepsilon_{\mathrm{imp}}$. This explains why the DFT magnetic moment does not always scale linearly with the charge transfer in Fig. 1(d). Detailed discussions are given in the SM [21].

The quantitative strength of the Kondo resonance is strongly modulated by the moiré superlattices forming between the molecular and the Pb lattices. Such moiré structures show long-range ordered super-periodicities and a tunable twist angle θ, both of which are absent in previous observations of the adsorption site dependent Kondo effect [27,36]. Figure 2(a–b) show three typical moiré superstructures with $\theta = 11°$, $\lambda = 10a_1$; $\theta = 13°$, $\lambda = 8a_1$; and $\theta = 17°$, $\lambda = 6a_1$ where λ represents the moiré periodicity along the $\vec{\boldsymbol{a}}_1$ direction. The upper panel in Fig. 2(c) shows a color rendering of the dI/dV spectra for 20 molecules along a bright row as labeled in Fig. 2(a). These dI/dV spectra can be fitted with the widely adopted Fano formula [25]. Representative spectra and the corresponding fits are displayed in Fig. S3(a). In the lower panel of Fig. 2(c), we show a plot of the half-width at half-maximum of the resonance (Γ) for each molecule. The peak value occurs at the location with the lowest topographic height (index #10 and #20), while the minimum value occurs at the highest locations (index #6 and #15). In all our measurements for the moiré superlattice with $\theta = 11°$, Γ varies from a minimum of 6.3 meV to a maximum of 20.5 meV, corresponding to a variation of T_{K} from 72 K to 238 K. A similar spatial mapping of the Kondo resonance for $\theta = 13°$ is displayed in Fig. S5. Both the oscillation amplitude (Γ

= 8.8 meV - 14.9 meV) and the average magnitude of Kondo screening are significantly smaller than that for $\theta = 11°$, demonstrating a twist-angle tuned Kondo screening for 2D impurity lattice. In this work, all spectra are acquired at the C-H bond location [21] when discussing the inter-molecular difference, unless stated otherwise.

When a single localized magnetic moment is coupled to a superconductor, its exchange interaction with the Cooper pairs leads to in-gap states, referred to as YSR bound states, after the seminal works of Yu, Shiba, and Rusinov [1-3]. Matsuura extended the original framework to include the Kondo screening and identified two regimes: (a) "free spin" regime ($\Gamma < \Delta$) where Kondo screening is quenched; and (b) "spin-screen" regime ($\Gamma > \Delta$) where the efficient Kondo screening leads to a singlet ground state. In the "spin screen" regime, the quasiparticle excitations are strictly not YSR states, albeit this distinction has been blurred in several recent literatures [46,47]. To avoid confusion, we simply refer to the quasiparticle excitations in the $\Gamma >> \Delta$ regime as "bound states" [40,48]. Exchange interactions of local moments and superconductors have gained tremendous interest lately. Nevertheless, most STS investigations have focused mainly on single magnetic impurities or impurity pairs [49-51]. Here we present a regime with the interaction of "Kondo screened delocalized 2D spin lattices" and the 2D superconductors where qualitatively different behaviors are observed.

Figure 3(a) shows dI/dV spectra (−4.0 mV to +4.0 mV) for three representative molecules [index #5, #6, and #10 in Fig. 2(c)] taken with an SC Nb tip at 0.4 K. These

spectra exhibit two sharp peaks (hole-particle symmetry in energy) each accompanied by a dip right next to them. By contrast, the spectrum acquired on the Pb surface does not exhibit such dips. After deconvolving of the Nb tip DOS [21], the sample DOS are displayed in Fig. 3(c). At first sight, these sample DOS resemble the pristine superconducting gap, except with smaller gap values. However, numerical analysis reveals that the presence of dips in Fig. 3(a) is related to spectral weight conservation, which manifests the formation of bound states [21]. In spectrum #10, the area of the apparent peak above the normalized reference line is marked as S_1 with the "absence" of spectral weight below the reference line denoted as S_2. The dip size is directly proportional to the ratio S_1/S_2. For a Bardeen-Cooper-Schrieffer (BCS) superconductor, spectral weight conservation ensures $S_1/S_2 = 1$; thus, no such dip would exist. The S_1/S_2 ratio represents the extent that the DOS deviates from the BCS line shape. The particle/hole quasiparticle excitation peaks are labeled as $\pm\Delta^*$, with Δ^* corresponding to the binding energy of the bound state.

A few important characteristics are noted: (i) the absence of multiplets typically observed for a high spin magnetic moment; (ii) a nearly symmetric particle/hole spectral weight; (iii) a spectral width broader than the typical bound state or YSR states; and (iv) a moiré modulation of Δ^* [Fig. 3(c)] which is in phase with the spatial moiré modulation of Γ [Fig. 2(c)]. Interestingly Γ *vs.* Δ^* (including more than 150 molecules over the surface) can be well-fitted with the theoretical model of Matsuura for $T_K >> \Delta$ [40]:

$$\Delta^* = \Delta_0 \frac{1-\alpha^2}{1+\alpha^2}, \text{ with } \alpha = \frac{\Delta_0}{\Gamma} \ln(\frac{\Gamma}{\Delta_0} \cdot e),$$

using an asymptotic value of $\Delta_0^{PTCDA/23ML}$ = 1.06 meV at $\Gamma = \infty$ [Fig. 3(d)]. Here Δ_0 is smaller than the gap value for 23ML Pb film (1.31 meV), suggesting that this hybrid 2D system has a reduced gap. The reduction in the SC gap is confirmed by the proximity effect [Fig. S9(c)], where the bare Pb surface experiences a gradual gap reduction as one laterally approaches a PTCDA island. We attribute this diminution of the SC order parameter to the finite magnetic impurity concentration, as proposed in the original model by Matsuura [48], which is beyond the YSR picture in the dilute limit.

The absence of multiplets in spectra acquired using a superconducting tip [Fig. 3(a)] simply reflects that our system is a 2D lattice comprised of quantum spins. The lack of particle/hole spectral weight asymmetry deserves some special attention. In most previous studies on bound states, the spectral weight between hole-like and electron-like quasiparticle excitations is highly asymmetric. In all our measurements, the present system comprised of π-electron magnetic moments, the particle/hole spectral weights are nearly symmetric, with a ratio of 0.93 in the most asymmetric case. Two controlling parameters influence the particle/hole quasiparticle spectral function [52]: the spin-exchange interaction (J) and Coulomb scattering potential (K_U), which contributes to the pair breaking and the particle-hole symmetry breaking, respectively [53]. Adopting the theory in Ref. [39, 54], we can extract J and K_U by analyzing Δ^* and the particle/hole spectral weight ratio (details in [21]). The moiré oscillations of $N_F|J|$ and $\frac{K_U}{|J|}$ are displayed in Fig.

2(d). The largest value of $\frac{K_U}{|J|}$ (~0.05) occurs at the location with the smallest gap, while on other sites, the values of $\frac{K_U}{|J|}$ are even smaller. The weak potential scattering is a characteristic feature of the magnetic moments residing in the relatively delocalized π-orbitals, yielding the nearly symmetric particle/hole spectral weights.

The delocalized nature of the spin-polarized orbital is also responsible for the broad spectral width (~0.5 meV in [21]) for the bound states. Further analysis is presented in Fig. S8, where the d*I*/d*V* spectra mapping with a fine step size shows that the bound states and Kondo resonance are continuous throughout the whole 2D interface, existing even on the sites between molecules. This is fundamentally different from the case of the MnPc/Pb system, where the bound states occur only on the Mn atoms [36]. Note that in the fitting of the Nb tip -Pb tunneling spectrum, small Dynes broadening parameters are used, and the effective temperature is determined as 0.63 K, which is close to the temperature reading (*i.e.*, 0.4 K) [21]. Thus, the large width of bound states can not be attributed to the instrumental energy resolution. As predicted in early theoretical works [3,55], an "impurity band" with a finite bandwidth of the bound states can form when the locally excited states can overlap with each other. Our observation suggests the formation of a 2D bound state band over the Kondo screened impurity lattice. The lateral coupling of the Kondo-screened bound states does not change the basic picture of the single-impurity Kondo effect until the moment concentration is of the same order of magnitude as the free carrier concentration [56]. We hope our discovery will inspire future theoretical efforts on this mixed regime.

Finally, we show that the quantum confinement effect (QCE) in Pb films can dramatically affect the Kondo/superconductivity interplay. Figure 4(a) shows large-energy-scale dI/dV spectra taken on 22ML and 23ML Pb films for both the bare Pb and PTCDA/Pb hybrid system. The thickness-dependent quantum well states are clearly seen [22,41,57,58]. The Γ values were 17.4 meV and 38.1 meV for the highest and lowest molecules within a moiré periodicity on 22ML Pb [Fig. 4(b)], which represents an enhancement by a factor of 2 in the Kondo screening energy and moiré modulation amplitude, compared with the results on 23 ML. The corresponding values of Δ^* were 0.97 meV and 1.16 meV, respectively [Fig. 4(c)]. The variation of Δ^* as a function of Γ on PTCDA/22ML-Pb yields an asymptotic $\Delta_0^{PTCDA/22ML}$ of 1.23 meV [Fig. 3(d)], which is significantly larger than the value of 1.06 meV for PTCDA/23ML Pb. The QCE only leads to a 3% change in SC transition temperature T_C between 22 ML and 23 ML bare Pb [21, 22]. After the Pb films were covered with a monolayer of PTCDA, the pairing strengths (fully Kondo-screened) show a difference of 15% (1.23 meV *vs.* 1.06 meV). This observation illustrates the complex and intriguing interfacial interplay in our system, where the thickness-dependent work function (and the DOS at E_F) [41] dictates the average magnetic moment and then determines the "impurity" concentration and the screening strength by the surrounding itinerant electrons [21], which in turn facilitates a much more effective tuning of the SC pairing strength.

In conclusion, we have established an unusual magnetism/superconductivity hybrid bilayer with pure π-electrons that are carrying the magnetic moments. Owing to the relatively delocalized nature of π–electrons, this hybrid system presents 2D-like behaviors for the interlayer stacking registry, the Kondo screening, and the bound state formation, which qualitatively distinguishes it from *d*-electron- and *f*-electron-based moment systems and thus opens new avenues for novel correlated physics. Moreover, the control over the twist angle offers a rare opportunity to explore the physics of the moiré modulated Kondo and superconductivity. In addition to combining moiré physics with quantum confinement effects, we demonstrated a practical tuning approach for the magnetic moment concentration and the SC pairing strength. Rich emergent quantum phenomena are anticipated with the combination of all these intriguing elements, as well as possibilities for fabrications of 2D organic structure [59] hosting topological and exotic fractionalized states.

We acknowledge funding from the National Science Foundation through the Center for Dynamics and Control of Materials: an NSF MRSEC under Cooperative Agreement No. DMR-1720595 and NSF Grant Nos. DMR-1808751, DMR-1949701, DMR-2114825; the Welch Foundation F-1672 and F-1841. We also acknowledge computing time from the Texas Advanced Computing Center. C.D.Z and H.-J.G thank the supports from the National Key R&D Program of China (Grant No. 2018FYA0305800 and 2018YFA0703700), the National Natural Science Foundation of China (Grant No.

11774268, 11974012 and 61888102), the Ministry of Science and Technology of China (No. 2013CBA01600) and the Strategic Priority Research Program of Chinese Academy of Sciences (Grant No. XDB30000000).

[1] L. Yu, Acta Phys. Sin. **21**, 75 (1965).
[2] A. I. Rusinov, P. M. Z. E. T. Fiz, JETP Lett **9**, 1101 (1968).
[3] H. Shiba, Prog. Theor. Phys. **40**, 435 (1968).
[4] X.-L. Qi and S.-C. Zhang, Rev. Mod. Phys. **83**, 1057 (2011).
[5] C. Nayak *et al.*, Rev. Mod. Phys. **80**, 1083 (2008).
[6] J. D. Thompson *et al.*, J. Magn. Magn. Mater. **226-230**, 5 (2001).
[7] F. Steglich and S. Wirth, Rep. Prog. Phys. **79**, 084502 (2016).
[8] O. V. Yazyev and M. I. Katsnelson, Phys. Rev. Lett. **100**, 047209 (2008).
[9] B. Trauzettel, D. V. Bulaev, D. Loss, and G. Burkard, Nat. Phys. **3**, 192 (2007).
[10] O. V. Yazyev, Rep. Prog. Phys. **73**, 056501 (2010).
[11] Z. Bullard, E. C. Girão, J. R. Owens, W. A. Shelton, and V. Meunier, Sci. Rep. **5**, 7634 (2015).
[12] R. R. Nair *et al.*, Nat. Phys. **8**, 199 (2012).
[13] H. González-Herrero *et al.*, Science **352**, 437 (2016).
[14] Y. Zhao *et al.*, J. Am. Chem. Soc. **142**, 18532 (2020).
[15] A. R. Carvalho, J. H. Warnes, and C. H. Lewenkopf, Phys. Rev. B **89**, 245444 (2014).
[16] W. L. Wang, O. V. Yazyev, S. Meng, and E. Kaxiras, Phys. Rev. Lett. **102**, 157201 (2009).
[17] S. Mishra *et al.*, Nat. Nanotechnol. **15**, 22 (2020).
[18] I. Fernández-Torrente, K. J. Franke, and J. I. Pascual, Phys. Rev. Lett. **101**, 217203 (2008).
[19] M. Garnica *et al.*, Nat. Phys. **9**, 368 (2013).
[20] T. Esat *et al.*, Nat. Phys. **12**, 867 (2016).
[21] See Supplemental Material at http://link.aps.org/supplemental for a description of the experimental methods and the DFT results, as well as additional experimental data and discussions, which includes Refs. [22–44].
[22] Y. Guo *et al*., Science **306**, 1915 (2004).
[23] S. Weiß *et al*., Nat. Commun. **6**, 8287 (2015).
[24] A. Kumar, K. Banerjee, and P. Liljeroth, Nanotechnology **28**, 082001 (2017).
[25] U. Fano, Physical Review **124**, 1866 (1961).
[26] M. Ternes, A. J. Heinrich, W.-D. Schneider, J. Phys. Condens. Matter **21**, 053001 (2008).
[27] Y. Jiang, Y. N. Zhang, J. X. Cao, R. Q. Wu, W. Ho, Science **333**, 324 (2011).
[28] Y. H. Zhang *et al*., Nat Commun **4**, 2110 (2013).
[29] D. Goldhaber-Gordon *et al*., Phys. Rev. Lett. **81**, 5225 (1998).
[30] M. Gruber, A. Weismann, and R. Berndt, J Phys Condens Matter **30**, 424001 (2018).

[31] H. Nam, *et. al*., Phys. Rev. B **100**, 094512 (2019).
[32] T. W. Odom, J.-L. Huang, C. L. Cheung, and C. M. Lieber, Science **290**, 1549 (2000).
[33] L. Farinacci *et al*., Phys. Rew. Lett. **125**, 256805 (2020).
[34] R. C. Dynes, V. Narayanamurti, J. P. Garno, Phy. Rev. Lett. **41**, 1509 (1978).
[35] F. Herman and R. Hlubina, Phys. Rev. B 94, 144508 (2016).
[36] K. J. Franke, G. Schulze, and J. I. Pascual, Science **332**, 940 (2011).
[37] A. Palacio-Morales *et al*., Science Advances **5**, eaav6600 (2019).
[38] S. Kezilebieke *et al*., Nature **588**, 424 (2020).
[39] M. I. Salkola, A. V. Balatsky, and J. R. Schrieffer, Phys. Rev. B **55**, 12648 (1997).
[40] T. Matsuura, Prog. Theor. Phys. **57**, 1823 (1977).
[41] J. Kim *et al*., P. Natl. Acad. Sci. USA **107**, 12761 (2010).
[42] G. C. Ménard *et al*., Nat. Phys. **11**, 1013-1016 (2015).
[43] J. Kim, *et al.*, Nat. Phys. **8**, 464-469 (2012).
[44] V. Cherkez *et al*., Phys. Rev. X **4**, 011033, (2014).
[45] T. Esat *et al*., Phys. Rev. B **91**, 144415 (2015).
[46] J. Bauer, J. I. Pascual, and K. J. Franke, Phys. Rev. B **87**, 075125 (2013).
[47] N. Hatter, B. W. Heinrich, D. Rolf, and K. J. Franke, Nat. Commun. **8**, 2016 (2017).
[48] T. Matsuura, S. i. Ichinose, and Y. Nagaoka, Prog. Theor. Phys. **57**, 713 (1977).
[49] S.-H. Ji, *et al*., Phys. Rev. Lett. **100**, 226801 (2008).
[50] S. Kezilebieke, *et al*., Nano Letters **18**, 2311 (2018).
[51] D.-J. Choi, *et al*. Phys. Rev. Lett. **120**, 167001 (2018).
[52] A. V. Balatsky, I. Vekhter, and J. X. Zhu, Rev. Mod. Phys. **78**, 373 (2006).
[53] B. W. Heinrich, J. I. Pascual, and K. J. Franke, Prog. Surf. Sci. **93**, 1 (2018).
[54] E. W. Hudson *et al*., Nature **411**, 920 (2001).
[55] Y. V. Fominov and M. A. Skvortsov, Phys. Rev. B 93, 144511 (2016).
[56] A. C. Hewson, *The Kondo Problem to Heavy Fermions* (Cambridge University Press, Cambridge, 1993), Cambridge Studies in Magnetism.
[57] T. Uchihashi, Supercond. Sci. Technol. 30, 013002 (2017).
[58] C. Brun, T. Cren, and D. Roditchev, Supercond. Sci. Technol. 30, 013003 (2017).
[59] D. Longo *et al*., J. Phys. Chem. C 124, 19829 (2020).

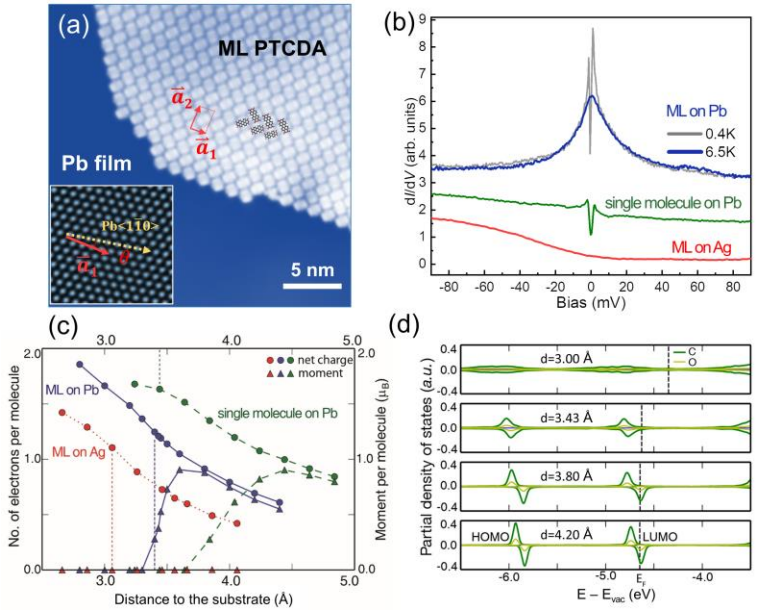

FIG. 1 (a) STM image of ML PTCDA/Pb film. The red rectangle represents a unit cell of the herringbone structure. The inset shows the atomically resolved image of the nearby Pb surface (4×4 nm^2). The twist angle θ is defined as labeled. (b) dI/dV spectra for the ML PTCDA/Pb, T_S = 0.4 K (gray) and 6.5 K (blue), a single molecule on Pb at 0.4 K (green), and the ML PTCDA on Ag(111) at 4.2 K (red). Spectra are shifted vertically for clarity. (c) The charge transfer and the magnetic moment as a function of the d for all three situations. The equilibrium distances are marked by vertical dashed lines. (d) Partial DOS at various d for ML PTCDA/Pb. The dashed lines indicate the Fermi levels (a) Sample bias V_s = 1.0 V, set-point current I = 25 pA. Setpoint in (b): V_s = 95 mV, I = 200 pA, and the lock-in modulation V_{rms} = 0.8 mV.

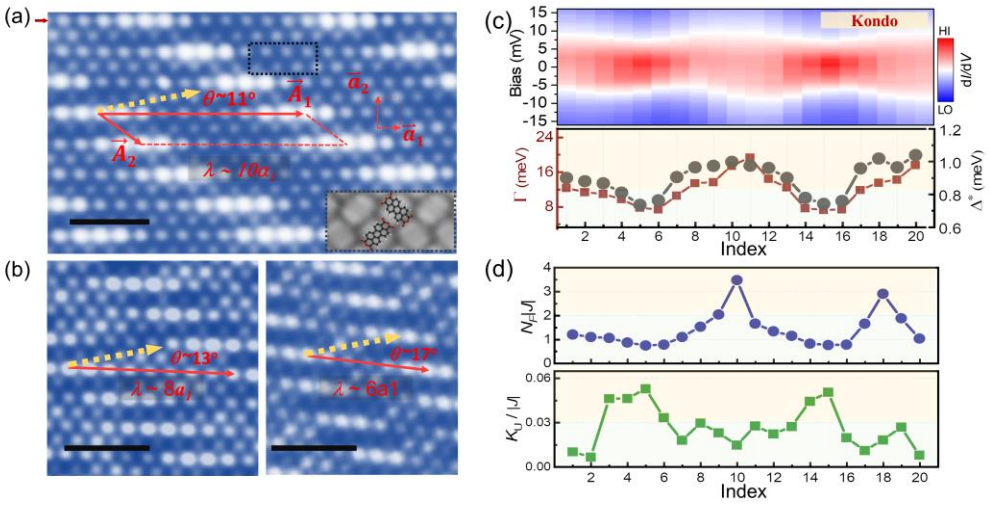

FIG. 2 (a)–(b) Typical Moiré superlattice for $\theta = 11^{\circ}$, $\theta = 13^{\circ}$, and $\theta = 17^{\circ}$. The red parallelogram in (a) represents the moiré supercell. λ is the periodicity along $\vec{a}_1$ direction. The Pb<$1\bar{1}0$> direction is marked by the yellow dashed arrow. Inset in (a) is a zoomed-in image at the black dashed rectangle with molecular models overlaid. (c) The upper panel is a false-color image of dI/dV spectra taken along the bright row marked in (a) by the red arrow. The lower panel shows the moiré modulations of Γ (wine) and Δ* (gray). A small magnetic field (0.5 T) was applied to quench superconductivity. (d) The corresponding oscillations of $N_F|J|$ (upper panel) and $K_U/|J|$ (lower panel). Spectra in (c) were taken at 0.4 K with $V_s = 95$ mV, $I = 100$ pA, $V_{rms} = 2.5$ mV. (a-b) $V_s = 2.0$ V, $I = 20$ pA; inset in (a) $V_s = 1.0$ V. Scale bars are 5.0 nm.

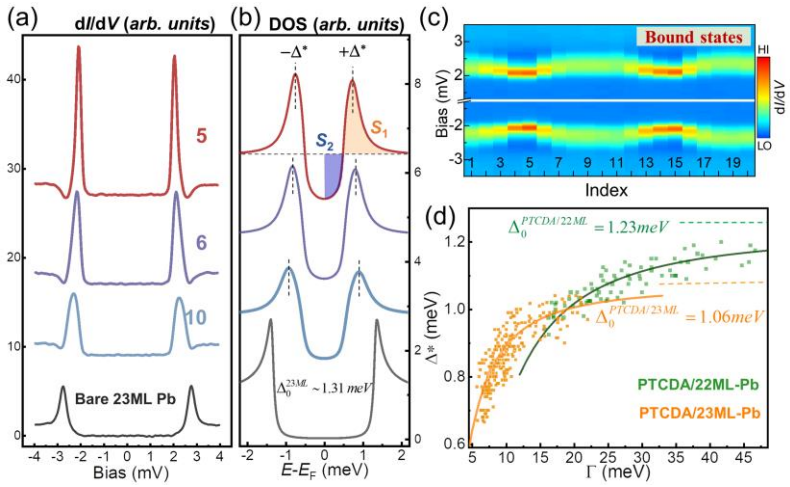

FIG. 3 (a) Pairing gap measurements for the molecule #5, #6 and #10 in the bright row in Fig. 2(a). (b) Sample DOSs obtained by numerical deconvolution of the superconducting tip DOS. Results of bare 23ML Pb are displayed for comparison. The peak area S_1, gap area S_2 and bound state energy level Δ^* are labeled as shown. (c) False-color image of the bound state measurements along the bright row in Fig 2(a). (d) Ensembles of data points on PTCDA/23ML Pb (orange) and PTCDA/22ML Pb (green), plotted in terms of the Δ^* versus Γ. The solid lines are fittings based on Matsuura's theory. The asymptotic limits of the SC order parameters at $\Gamma = \infty$ are labeled. All spectra were taken by Nb tips at 0.4 K. $V_s = 4.0$ mV, $I = 100$ pA, $V_{rms} = 50\mu$V.

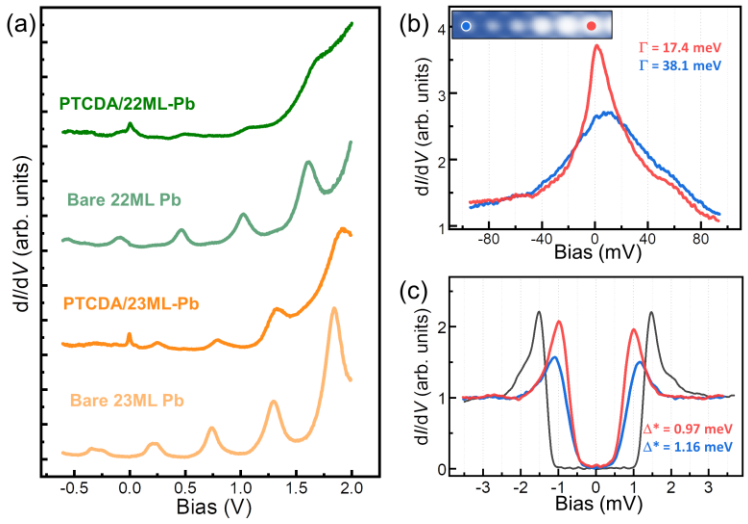

FIG. 4 (a) d*I*/d*V* spectra from -0.6 V to +2.0 V taken on the ML PTCDA/22 ML Pb, bare 22 ML, ML PTCDA/23 ML Pb, and 23 ML Pb surfaces. (b) and (c) Measurements of Kondo resonances and pairing gaps on ML PTCDA/22 ML Pb. Two typical spots are chosen: the morphologically highest (red) and lowest (blue) molecules within one moiré periodicity [labeled in the inset of (b)]. The black curve in (c) is taken on bare 22 ML Pb with its SC gap Δ_0^{22ML} =1.35 meV [21]. All spectra were taken at 0.4 K with a normal tip. (b) V_s = 95 mV, I = 100 pA, V_{rms} = 2.5 mV; (c) V_s = 3.5 mV, I = 100 pA and V_{rms}= 50 μV.